Charge Transfer Time in Alkanethiolate Self-Assembled Monolayers via Resonant Auger Electron Spectroscopy

ARTICLE *in* THE JOURNAL OF PHYSICAL CHEMISTRY C · JULY 2010

Impact Factor: 4.77 · DOI: 10.1021/jp1042816

5 AUTHORS, INCLUDING:

Stefan Neppl
Lawrence Berkeley National Laboratory
30 PUBLICATIONS **616** CITATIONS
SEE PROFILE

David L Allara
Pennsylvania State University
261 PUBLICATIONS **23,054** CITATIONS
SEE PROFILE

Charge Transfer Time in Alkanethiolate Self-Assembled Monolayers via Resonant Auger Electron Spectroscopy

Ping Kao,[†] Stefan Neppl,[‡] Peter Feulner,[‡] David L. Allara,[†] and Michael Zharnikov*[,§]

Departments of Chemistry and Material Science, Pennsylvania State University, University Park, Pennsylvania 16802, Physik Department E20, Technische Universität München, D-85747 Garching, Germany, and Angewandte Physikalische Chemie, Universität Heidelberg, D-69120 Heidelberg, Germany

Received: May 11, 2010; Revised Manuscript Received: July 8, 2010

The dynamics of the charge transfer (CT) in alkanethiolate self-assembled monolayers is addressed by resonant Auger spectroscopy using the core hole clock method. The CT pathway was unambiguously defined by resonant excitation of the nitrile tailgroup attached to the alkyl backbone. The length of this backbone was varied to monitor the respective dependence of the CT time. It was found that, similar to the static conductance, this dependence can be coarsely described by an exponential function with an attenuation factor of 0.93 per methylene unit (0.72 $Å^{-1}$; a tunneling along the chain was assumed). As a result, the CT time is quite long even for a relatively short alkyl chain; in particular, it is ca. 100 fs for the chain consisting of only four CH_2 units. In contrast, the CT time associated with the thiolate headgroup anchor was found to be quite short, viz. 2.3 fs, which suggests an efficient interfacial electronic coupling between the aliphatic backbone of the C*n*CN molecules and the substrate over the thiolate−gold linkage.

1. Introduction

The emergence of molecular and organic electronics as frontier fields of modern science and technology requires reliable experimental data regarding the charge transport (CT) in individual molecules and their functional units.[1−10] In particular, in the framework of molecular electronics one can imagine a future molecular "device" as consisting of an active group which can be addressed, for example, by light or electrochemically, and an anchor group which is responsible for the attachment of the entire molecule to a bottom electrode. The direct contact to or even close vicinity of such a conductive electrode can, however, disturb the performance of the active group so that its decoupling from the substrate may be necessary. This can be easily achieved by introduction of a chain-like molecular spacer (wire) between the active moiety and the headgroup. Within the resulting architecture, the transport characteristics of this wire as well as the coupling efficiency of the anchor-group-electrode linker will influence the performance of the entire device.

In view of the above challenges, significant activity regarding the investigation of the transport properties of potential molecular wires and prototype molecules assembled in different fashions on conductive substrates has evolved.[6] A variety of different experimental setups have been developed, including conducting probe AFM- and STM-based approaches,[11−18] break junction techniques,[19−24] in-wire junctions,[23] mercury drop methods,[25−27] etc. However, in spite of the sophisticated setups, it is difficult to control the number of molecules participating in the current transport on one side and the exact shape of the nanoelectrodes on other side, which, according to theory, dramatically influences the CT properties.[28,29] This makes it complicated to untangle the contribution of the individual molecule from the integral $I-V$ curves of a particular junction. Nevertheless, a variety of valuable experimental data has been collected. In particular, it has been shown that the current J through a metal−molecule−metal junction can in most cases, and always when coherent tunneling is the relevant mechanism, be described by an exponential function, $J = J_0 \exp(-\beta d)$, with d being the molecular length and β a decay factor.[6,11,13,18,26,30] A pre-exponential factor J_0 is closely related to the contact resistance which in turn is determined by the molecule−substrate bonding and overlap of electronic states at the junction (see, e.g., refs 15 and 18). An attenuation factor β depends primarily on the identity of the molecular wire (see, e.g., refs 6 and 11) but is also influenced by some other factors, e.g., the exact positions of the HOMO and LUMO with respect to the Fermi level of the electrodes,[18] the local molecular environment,[23] etc.

All the above knowledge and results refer, however, to the static properties of a metal−molecule−metal junction, whereas the quantitative dynamics of CT through potential molecular wires and prototype molecules assembled on or between conductive electrodes has been largely unexplored. Recently, we demonstrated that the CT dynamics phenomena in the above systems can be successfully addressed by resonant Auger electron spectroscopy (RAES) using the core hole clock (CHC) method.[31] This contact-free approach is based on the fact that the core hole decay spectra obtained for resonant excitations of core-to-bound states differ for decay events *before* and *after* the transfer of the resonantly excited electron to the substrate.[32] Under suitable conditions, such spectra can be decomposed into the contributions related to these two scenarios and the CT time (τ_{CT}) is obtained from the relation $\tau_{CT} = \tau_{core}\,(1 - P_{CT})/P_{CT}$, where τ_{core} is the known lifetime of inner-shell vacancy (see, e.g., ref 33) and P_{CT} is the integrated post-CT portion of the decay spectrum.[32] Thus, τ_{core} is used as an internal time reference, core hole clock, for the CT time. Previously, the CHC method has been applied to organic films on different substrates (see, e.g., refs 34−37) including nonfluorinated and partly

* To whom correspondence should be addressed. Phone: +49-6221-54 4921. Fax: +49-6221-54 6199. E-mail: Michael.Zharnikov@urz.uni-heidelberg.de.
[†] Pennsylvania State University.
[‡] Technische Universität München.
[§] Universität Heidelberg.

10.1021/jp1042816
Published on Web 07/23/2010

fluorinated terphenylthiols[37] and prototype molecular electronics moieties such as thiolate-bonded oligophenylene−ethylynene (OPE) chains[36] on gold for which different OPE derivatives lead to fast switching, rectification, and negative differential resistance.[7] For the simple OPE-type structures, in previous work a resonant excitation of the carbon atoms comprising the molecular backbone was performed and backbone-to-substrate CT measured.[36] The respective CT was found to occur extremely fast, even below the time region accessible with resonant C1s excitations.[36] However, since the excitation site in terms of a distinct carbon atom on the molecular wire was not defined, the CT pathway was not well-defined either. One therefore cannot exclude that the entire pattern is related to the carbon atom adjacent to the thiolate group, so that the very fast CT is exclusively related to the thiolate−gold anchor.

To avoid such ambiguity, we defined the CT pathway precisely by attachment of a specific group, which could be resonantly excited by X-rays, to the molecular backbone and measured the CT time from this tail group to the substrate, through the backbone, and across the headgroup−substrate anchor.[31] As a test system we used the archetypical system of self-assembled monolayers (SAMs) of alkanethiols on Au(111),[38−40] and for a tail group we used nitrile. This group can be resonantly excited by narrow bandwidth synchrotron radiation at both C and N K-edges, with the latter option being preferable since the alkyl backbone is nitrogen free and therefore does not contribute to the respective RAES spectra. In our first experiments we studied SAMs comprised of quite short ($CN(CH_2)_2SH$) and quite long ($CN(CH_2)_{16}SH$) molecules abbreviated below as C2CN and C16CN, respectively. For the latter SAM, no traces of CT have been found in the N 1s core hole decay spectrum. In contrast, a pronounced CT contribution appeared in the analogous spectrum of C2CN SAM, and the CT time between the tail group and the substrate could be estimated at 15 ± 4 fs.[31] Since the portion of the CT curve in the entire N 1s core hole decay spectrum was quite high (ca. 30%), there was a hope that this contribution can be traced for the longer molecules as well.

On the basis of this assumption, in the present study we applied the CHC approach to a series of nitrile-substituted short-chain alkanethiols of different lengths and monitored the dependence of the respective CT time on the chain length. Since the preparation and handling of such short-chain SAMs requires special care, we placed particular attention on characterization of these films to check their identity and prove their integrity. Only in the case of high-quality films, the results of the CHC experiments can be considered as reliable.

In the following we provide a brief description of the experimental procedure and setup. Thereafter, results are presented and explained in section 3. More detailed discussion is given in section 4. Finally, the results are summarized in section 5.

2. Experimental Section

The target compounds for the SAM preparation were $CN(CH_2)_2S-S(CH_2)_2CN$ and $CN(CH_2)_nSH$ with $n = 3$, 4, and 16. Considering that the disulfide and thiol bonds will be cleaved upon adsorption, all respective SAMs will be abbreviated similarly as C*n*CN below. 3,3′-Dithiobis(propionitrile) was purchased from Aldrich and recrystallized by a mixture of ethanol and water. 4-Mercaptobutyronitrile and 5-mercaptovaleronitrile were synthesized from 4-bromobutyronitrile and 5-bromovaleronitrile (Aldrich), respectively, by adopting the method previously reported in ref 41, The synthesis of C16CN is described in ref 42. The gold substrates were prepared by thermal evaporation of 150 nm of gold (99.99% purity) onto polished single-crystal silicon (100) wafers (Silicon Sense) primed with a 10 nm chromium adhesion layer. The resulting metal films were polycrystalline, with grains exhibiting predominantly the (111) orientation and a size of 20−50 nm. The SAMs were prepared by immersion of the freshly prepared substrates into a 1 mM solution of the target compounds in anhydrous ethanol at room temperature for 24 h. After immersion, the samples were carefully rinsed with pure solvent and blown dry with argon. Afterward, they were put into glass containers and stored there under inert gas atmosphere until characterization at the synchrotron (see below).

The spectroscopic experiments were performed at the bending magnet beamline D1011 at the MAX II storage ring of the MAX-lab synchrotron radiation facility in Lund, Sweden. All experiments were carried out at room temperature and under UHV conditions at a base pressure of less than 2×10^{-10} mbar. The photon dose was limited to a value that was small enough to avoid any noticeable beam damage.[43−46] In most cases, several different spots at the surface of each sample were used to minimize the X-ray load for the individual spectra.

The physical and chemical integrity of the C*n*CN SAMs were controlled by high-resolution X-ray photoelectron spectroscopy (HRXPS) and near-edge X-ray absorption fine structure (NEXAFS) spectroscopy.

The HRXPS spectra were acquired in the normal emission geometry using a SCIENTA SES200 electron energy analyzer. The energy resolution was better than 100 meV, allowing a clear separation of individual spectral components. The binding energy (BE) scale of every spectrum was individually calibrated using the Au $4f_{7/2}$ emission line of the underlying Au substrate at 83.95 eV.[47] HRXPS spectra were fitted by symmetric Voigt functions and a Shirley-type background. To fit the S $2p_{3/2,1/2}$ doublet we used two peaks with the same full width at half-maximum (fwhm), the standard[48] spin−orbit splitting of ∼1.18 eV (verified by fit), and a branching ratio of 2 ($S2p_{3/2}/S2p_{1/2}$).

NEXAFS spectra were collected in the partial electron yield (PEY) mode using a multichannel plate detector. Spectra were acquired at the carbon and nitrogen K-edge using retarding voltages of −150 and −300 V, respectively. Linearly polarized synchrotron light with a polarization factor of ∼95% was used. The energy resolution was better than 100 meV. The incidence angle of the light was varied from 90° (**E** vector in the surface plane) to 20° (**E** vector nearly normal to the surface) in steps of 10°−20° to monitor the orientational order of the C*n*NC molecules within the films. This approach is based on the linear dichroism in X-ray absorption, i.e., the strong dependence of the cross-section of the resonant photoexcitation process on the orientation of the electric field vector of the linearly polarized light with respect to the molecular orbital of interest.[49]

The raw NEXAFS spectra were normalized to the incident photon flux by division through a spectrum of a clean, freshly sputtered gold sample. Further, the spectra were reduced to the standard form by subtracting the linear pre-edge background and normalizing to the unity edge jump (determined by a nearly horizontal plateau 40−50 eV above the respective absorption edges). The photon energy (PE) scale was referenced to the most intense π^* resonance of highly oriented pyrolytic graphite (HOPG) at 285.38 eV.[50] For the absolute energy calibration of the N K-edge NEXAFS spectra, we utilized the apparent shift in the position of the Au $4f_{7/2}$ core level of a clean Au wafer on going from the beamline settings used for the C K-edge NEXAFS data collection to those for the N K-edge; a similar approach was used at the measurement of NEXAFS spectra of

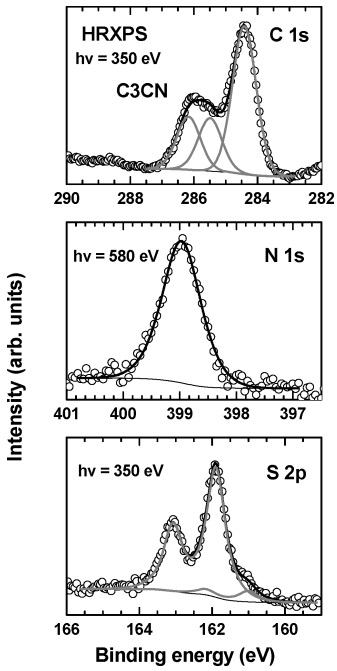

Figure 1. C 1s, N 1s, and S 2p HRXPS spectra of C3CN/Au (hollow circles), representative of the entire CnCN/Au series. C 1s and S 2p are decomposed into several components (gray lines). Background is shown (thin black lines).

proteinogenic α-amino acids and nucleobases.[51,52] The resultant energy positions are expected to be accurate and reproducible within ±0.05 eV.

The resonant and nonresonant Auger spectra (decay electron signal) were acquired using a SCIENTA SES200 electron energy analyzer. The X-ray incidence angle was set to 55° (magic angle; see above); the take-off angle of the electrons was close to normal emission. The resonant excitation energies were determined by preliminary NEXAFS measurements. For every sample, an additional spectrum for the pre-edge excitation was also recorded. This spectrum was subtracted from the RAES and nonresonant AES spectra to correct them for contributions of subthreshold photoemission from orbitals with lower binding energy.

3. Results

3.1. HRXPS and NEXAFS Spectroscopy Characterization. C 1s, N 1s, and S 2p HRXPS spectra of C3CN/Au are depicted in Figure 1, representative of the entire C*n*CN/Au series. The C 1s spectrum exhibits a peak at a BE of ∼284.4 eV and a broad plateau-like shoulder at higher BE. In view of the chemical structure of C3CN, the spectrum can be decomposed into three peaks at ∼284.4, ∼285.5, and ∼286.2 eV, assigned to the two "inner" carbon atoms in the alkyl chain, the carbon atom adjacent to the nitrile group, and nitrile carbon, respectively. In addition, the ∼284.4 eV peak can contain a contribution of hydrocarbon contamination, which could not be avoided completely because of the limited self-cleaning ability of the relatively short target molecules. A very weak trace of another, oxygen-containing contamination is seen at a BE of ∼288.7 eV.

The N 1s spectrum of C3CN/Au exhibits a single emission at 398.98 eV related to the nitrile nitrogen. The BE of this emission increases continuously on going from C2CN/Au to C16CN/Au as shown in Figure 2, in which the N 1s spectra of the entire C*n*CN series are depicted. This behavior can be

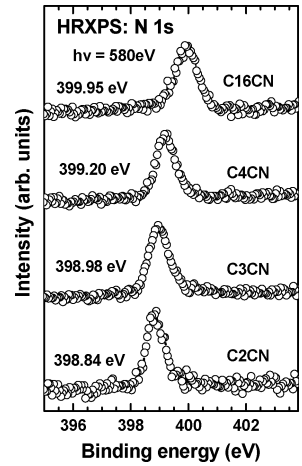

Figure 2. N 1s HRXPS spectra of C2CN/Au, C3CN/Au, C4CN/Au, and C16CN/Au (hollow circles). The BE positions of the emission are given at the respective curves.

tentatively associated with screening of the N 1s photoemission hole by the conduction electrons in the substrate (image charge). The extent of this effect depends on the distance between the excitation site and the substrate and is stronger for the shorter molecules, resulting in the lower BE of the N 1s emission. Note that the lack of splitting of the N 1s emission and its continuous shift correlating with the molecular length confirm that all nitrile groups in the C*n*CN SAMs of this study are located at the SAM−ambient interface.

The S 2p spectrum of C3CN/Au in Figure 1 exhibits a single doublet at a BE of ∼161.9 eV. This doublet can be clearly assigned to thiolate species bonded to the surfaces of the gold substrate.[53−56] No features related to physisorbed molecules or oxidized C3CN molecules could be recognized, which means that all the C3CN molecules in the SAM are anchored to the substrate in a thiolate-like fashion. One should note, however, that a detailed analysis of the spectrum suggests the presence of an additional, low-intensity doublet at a BE of ∼161.0 eV (S $2p_{3/2}$). This feature can be ascribed either to atomic sulfur[57] or a thiolate-type bound sulfur with a different binding chemistry and/or geometry as compared to the "standard" thiolate-type bond observed in thiol-derived SAMs on coinage metal substrates.[54,58] Both assignments are discussed in detail in refs 59 and 60, but we would like to note here that in most situations involving SAMs, including the present case, a "different thiolate" assignment can be favored.

The C and N K-edge NEXAFS spectra of C2CN/Au, C3CN/Au, C4CN/Au, and C16CN/Au acquired at an X-ray incident angle of 55° are presented in Figures 3 and 4, respectively, along with the difference between the spectra of C3CN/Au acquired at X-ray incident angles of 90° and 20°, representative of the entire C*n*CN/Au series. An angle of 55° is the so-called magic angle of X-ray incidence; at this particular geometry, the spectrum is not affected by any effects related to molecular orientation and gives only information on the chemical identity of investigated samples.[49] Molecular orientation is monitored by the difference spectra.

The C K-edge spectra in Figure 3 exhibit an absorption edge related to C 1s → continuum excitations and several pronounced π^* and σ^* resonances. The assignments of these resonances can be found in ref 42. The spectra are dominated by a distinct $\pi^*(C^*{\equiv}N^*)$ resonance at a PE of 286.8−286.9 eV. This resonance becomes more intense on going from C2CN/Au to C4CN/Au, following the improving film quality, but saturates with increasing number of carbon atoms in the target molecule

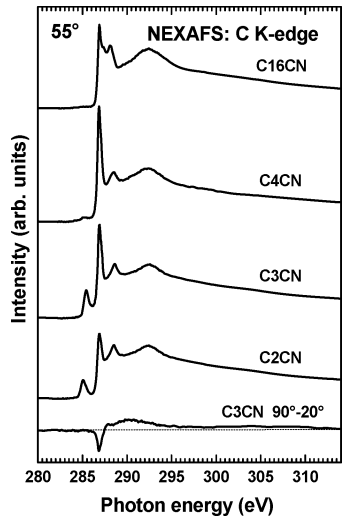

Figure 3. Carbon K-edge NEXAFS spectra of C2CN/Au, C3CN/Au, C4CN/Au, and C16CN/Au acquired at an X-ray incident angle of 55° along with the difference between the spectra of C3CN/Au acquired at X-ray incident angles of 90° and 20° (bottom curve; representative of the entire C*n*CN/Au series).

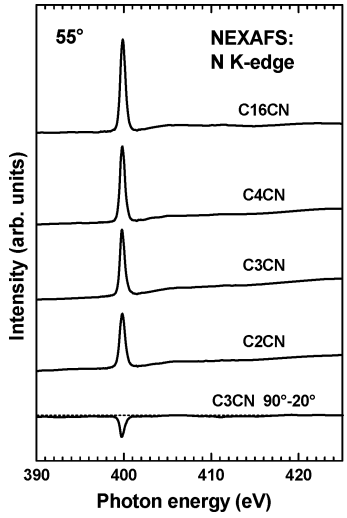

Figure 4. Nitrogen K-edge NEXAFS spectra of C2CN/Au, C3CN/Au, C4CN/Au, and C16CN/Au acquired at an X-ray incident angle of 55° along with the difference between the spectra of C3CN/Au acquired at X-ray incident angles of 90° and 20° (bottom curve; representative of the entire C*n*CN/Au series).

as emphasized by the spectrum of C16CN/Au. This feature is accompanied by a R*/C−H σ* resonance at ∼288.0 eV assigned to the alkyl chain;[61,62] the latter resonance is distinctly pronounced only for C16CN/Au, weak for C4CN/Au, and hardly visible for C3CN/Au and C2CN/Au. Such a behavior is explained by the fact that the intensity of the R*/C−H σ* resonance depends on the alkyl chain length, growing significantly with increasing length due to delocalization of the respective molecular orbital over the entire chain.[63,64] A pronounced feature at ∼288.5 eV, visible only in spectra of the short-chain C*n*CN SAMs is presumably related to the nitrile group (a σ* resonance) but can also contain some contribution from the π*(C*≡O) resonance associated with possible contamination. In our experience, the oscillator strength of the latter resonance is comparably high, so that it becomes distinctly visible even if contamination is small. A further signature of contamination is a π*(C═C) resonance at 285.0 eV. It is comparably strong for C2CN/Au and C3CN/Au, weak for C4CN/Au, and not perceptible for C16CN/Au.

TABLE 1: Binding Energies of the N 1s Emission (eV), Excitation Energies of the [N1s]π* Resonance (eV), and Their Difference (eV) for the Target SAMs of this Study

	C2CN	C3CN	C4CN	C16CN
[N1s]	398.84	398.98	399.20	399.95
[N1s]π*	399.75	399.75	399.75	399.75
[N1s]π*−[N1s]	+0.91	+0.77	+0.55	−0.2

This difference represents the energy of the π*-resonantly excited N 1s electron at the nitrile group with respect to the Fermi energy of the substrate (E_{res}).

The N K-edge spectra of the C*n*CN SAMs in Figure 4 exhibit a single π*(C≡N*) resonance. Similar to the C K-edge, the positions of this resonance, which is a neutral excitation, differ only marginally for the C*n*CN samples of this study. The intensity of the π*(C≡N*) resonance increases to some extent with increasing molecular length following the film quality.

As follows from the 90°−20° difference spectra in Figures 3 and 4, both π*(C*≡N) and π*(C≡N*) resonances exhibit a clear linear dichroism, which suggests that the −CN moieties in the C*n*CN monolayers exhibit a uniform orientation. Since the respective molecular orbital is perpendicular to the bond direction, the negative sign of the π*(C*≡N) and π*(C≡N*) difference peaks suggests that the nitrile group is strongly inclined. The respective tilt angle was estimated at 65° for C16CN,[42] and in view of the comparable dichroism, it is presumably similar for the further SAMs of this study. Note that such an in-plane orientation of the nitrile groups in the C*n*CN SAMs is likely related to minimization of the comparably strong electrostatic interaction between these dipolar groups at the SAM−ambient interface.[42,65]

3.2. CHC Measurements. The results of the spectroscopic characterization suggest that all the C*n*CN SAMs of this study exhibit a significant degree of self-organization, high purity, and uniform orientation with all molecules bound to the substrate by the thiolate−gold anchor. All nitrile groups are located at the SAM−ambient interface and do not have direct contact to the substrate. Thus, the CT pathway to the substrate at the resonant excitation of the nitrile group is unequivocally defined. However, CT to the substrate can only occur if it is energetically allowed. For this, the energy of the π*-resonantly excited electron at the nitrile group, E_{res}, should be positive with respect to the Fermi level of the substrate. The values of E_{res} can be estimated by comparison of the binding energies of the N 1s emission and the excitation energies of the [N1s]π* resonance. Such a comparison and evaluation of E_{res} is performed in Table 1. According to this table, the tailgroup-to-substrate transfer of the resonantly excited electron is energetically allowed for C2CN/Au, C3CN/Au, and C4CN/Au, while it is forbidden for C16CN/Au, where we can only expect the reverse process, i.e., substrate-to-tailgroup neutralization of the core ionized state.

As mentioned in section 1 and illustrated in Figure 5, decay of this excitation can occur in three possible ways if radiative decay is neglected. First, the excited electron itself can be emitted while another valence electron fills the core vacancy. This so-called participator (P) scenario results in a final state with one hole in the OV region. Second, the excited electron stays in the UV states and two other OV electrons fill the hole and are emitted, respectively. This so-called spectator (SP) scenario results in a final state with two holes in the OV states but an additional electron in the UV states, giving in integral one hole per excited atom. Third, CT of the excited electron to the CB of the substrate can occur, followed by the standard Auger decay. This route leads to the final state with two holes

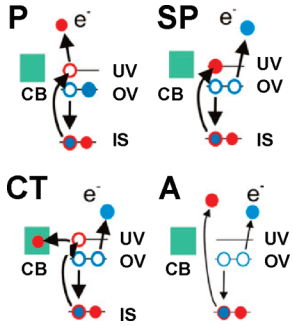

Figure 5. Scheme of core excitation/de-excitation routes in a functional group weakly coupled to a continuum (substrate conduction band, CB), with IS, OV, and UV denoting inner shell, occupied, and unoccupied valence levels, respectively. Following excitation of a core electron (curved arrow) into a bound state, either the excited electron itself (UV) or another, OV electron can be emitted, described as participator (P) and spectator (SP) decay, respectively. Both processes result in characteristic final states with one hole in OV. Alternatively, charge transfer (CT) of the excited electron to CB can occur. This route leads to the same final state with two holes in OV as a nonresonant Auger process (A). The letter process involves excitation of a core electron into a continuum state (curved arrow) followed by emission of an OV electron. The hole in IS is in every case filled by the electron transition from OV.

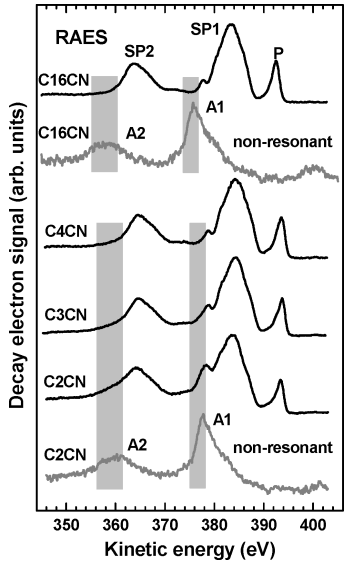

Figure 6. [N1s]π^* RAES spectra of C2CN/Au, C3CN/Au, C4CN/Au, and C16CN/Au (black curves) along with nonresonant AES spectra of C2CN/Au (representative of C3CN/Au and C4CN/Au as well) and C16CN/Au (gray curves). P, SP1, and SP2 denote the participator and two spectator features. A1 and A2 denote two characteristic features in the nonresonant spectra. The kinetic energy ranges where a contribution from these features in the RAES spectra can be expected are highlighted by light gray.

in OV, which is identical to the final state of the Auger decay in the case of nonresonant excitation. Due to the different and differently charged final states, the features related to the above scenarios can be distinguished in the joint RAES spectrum as far as the target group is clearly defined and the resonant excitation does not interfere too much with the contributions from other excitation routes (e.g., photoemission) or other functional groups within the molecule.

Such a favorable situation exists for the nitrile group in C*n*CN/Au. The [N1s]π^* RAES spectra of C2CN/Au, C3CN/Au, C4CN/Au, and C16CN/Au are presented in Figure 6 along with the nonresonant AES spectrum of C2CN/Au, representative of the entire series. In perfect agreement with data from condensed[66] and gaseous acetonitrile and calculations[66,67] and our own previous results for C2CN/Au and C16CN/Au,[31] we obtained for all C*n*CN SAMs nonresonant Auger spectra with two broad maxima A1 and A2 that have been assigned to final states with double holes in outer (A1) and holes in outer as well as inner valence orbitals (A2).[66−68] These maxima are observed around 378 and 360 eV for C2CN/Au, slightly lower kinetic energies (KEs) for C3CN/Au and C4CN/Au and ∼3 eV lower energies for C16CN/Au. This behavior is related to enhanced substrate-induced screening of the respective 2-hole states in the thinner films. For the [N1s]π^* resonant excitation, A1 and A2 turn into the blue-shifted 2-hole, 1-electron spectator peaks SP1 and SP2. In addition, the 1-hole participator line P appears. The KE positions of these features shift downward only slightly with increasing chain length since the screening effect in the case of 2-hole 1-electron states (SP1 and SP2) or 1-hole state (P) is smaller than in the case of the 2-hole states (A1 and A2).

For resonant excitation, CT before core decay results in an admixture of nonresonant decay signatures to the purely resonant spectrum.[32] Considering the relative positions of the SP1, SP2, A1, and A2 features, such an admixture results in the appearance of an additional signal at the low KE flanks of both SP1 and SP2 peaks. For C16CN/Au no contributions of A1 and A2 are visible in this case of resonant excitation, as expected in view of the energetic constraints (see above) and in agreement with our previous results.[31] The small maximum of SP1 at ∼378 eV differs from A1 by more than 3 eV and is much narrower. It is a specific feature of the autoionization spectrum and does not indicate tailgroup−substrate electron transfer for C16CN/Au.

In contrast to C16CN/Au, for the short-chain SAMs of this study, A1 and A2 clearly contribute to the RAES spectra, indicating charge transfer before core decay. This contribution seems to decrease with increasing chain length. In order to quantify the spectral composition, we fitted the resonant decay spectra of C2CN/Au, C3CN/Au, and C4CN/Au by a linear combination of their nonresonant counterparts and the blue-shifted resonant decay spectrum of C16CN/Au, which we assume to represent the "pure" autoionization spectrum of the CN group. The results for C2CN/Au are very close to those in ref 31: a combination of 31% nonresonant and 69% resonant spectra reproduces the π^*-resonant C2CN/Au decay spectrum within a small error (30% and 70%, respectively, in ref 31). The fittings of the [N1s]π^* RAES spectra of C3CN/Au and C4CN/Au are shown in Figure 7. The portions of the resonant spectra corresponding to the best fits were found to be 84.5% and 94% for C3CN/Au and C4CN/Au, respectively. For the above values and a N1s lifetime of 6.4 fs,[69] we obtain 14 ± 4, 35 ± 9, and 100 ± 26 fs for the transfer time τ_{CT} of the resonantly excited electron from the CN tail group of the C2CN, C3CN, and C4CN molecules, respectively, to the substrate. The error is mainly due to uncertainties of the core hole lifetime (cf., e.g., refs 33 and 69). However, for C4CN/Au, the error is presumably even larger because of the limited accuracy of the fitting procedure at the comparable small (just 6%) CT contribution; here we approach a limit of the CHC method. Note that for another, independently prepared C2CN/Au sample, which we studied in the course of the experiments, we got a value of 16.5 ± 4 fs for τ_{CT}. The average core hole lifetime of 15.25 fs is almost identical with our previous value of 15 ± 4 fs[31] obtained with different samples at the different synchrotron radiation facility (BESSY II in Berlin). This agreement underlines the reliability of the experiments. At the same time, for the C3CN/Au samples, which proved to be especially difficult

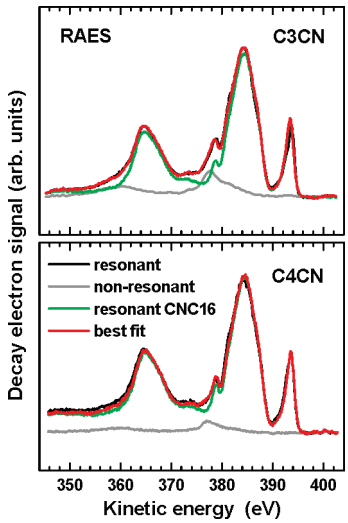

Figure 7. [N1s]π^* RAES spectra (black lines) of C3CN/Au (top) and C4CN/Au (bottom) along with the respective nonresonant AES spectrum (gray lines), RAES spectrum of C16CN/Au (green lines), and linear combination of the latter two spectra (red lines). The weighting factors were optimized to reproduce the [N1s]π^* RAES spectra of C3CN/Au and C4CN/Au. The RAES spectrum of C16CN/Au was shifted by ~0.7 eV.

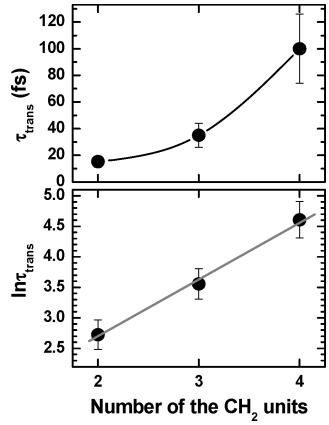

Figure 8. CT time (top) from the excited nitrile group to the substrate and its natural logarithm (bottom) versus the number (n) of the CH_2 units in the aliphatic chain of CnCN/Au (black filled circles). The gray solid line in the bottom panel represents the best fit.

to prepare and keep intact, we observed a variation of τ_{CT} depending on the sample quality. The above value of 35 ± 9 fs corresponds to a high-quality sample, whereas for low-quality samples a τ_{CT} value of 26 fs was obtained. In the given case, due to the significant difference in the sample quality, we refrain from averaging and consider 35 ± 9 fs as being representative of C3CN/Au.

4. Discussion

The derived values of τ_{CT} are shown in the top panel of Figure 8 versus the number (n) of CH_2 units in the aliphatic chain of CnCN/Au. The observed dependence is distinctly nonlinear. Considering the analogous relation for the conduction of the aliphatic chain (see section 1), it is logical to calculate the natural logarithm of τ_{CT}. The respective results are presented in the bottom panel of Figure 8. Similarly to the conductance case, we obtain a dependence of τ_{CT} on n which, within the error of the experiments, is very close to the linear function, as demonstrated by the best-fitting line. The slope and intercept points corresponding to the best fit are 0.93 (0.72 $Å^{-1}$; a tunneling along the chain was assumed;[70] see ref 71 for discussion on possible CT pathways) and 0.83, respectively. The former value can be considered as an analogue of the attenuation factor β in the conductance formula. Significantly, our value (β_{CT}) is very close to β for conductance, which was evaluated at 0.9−1 per CH_2 unit.[6,26] As for the intercept point value, it should correspond to the CT time through the thiolate−gold anchor; 0.83 for ln $\tau_{thiolate}$ gives a $\tau_{thiolate}$ of 2.3 fs. This suggests an efficient interfacial electronic coupling between the aliphatic backbone of the CnCN molecules and the substrate over the thiolate−gold linkage, which is in qualitative agreement with the previous CHC results for thiolate-bonded nonfluorinated and partly fluorinated terphenyl and phenylene−ethylynene chains on gold.[36,37] In the latter studies the C 1s core electron of one of the carbon atoms comprising the fluoro- or hydrocarbon backbone was excited and a decay of the excited state was monitored. Since the excited carbon atom could not be distinguished from the other carbons, the CT part of the resonant photoelectron spectra was presumably mediated by the carbon atom adjacent to the thiolate group; the CT from this atom to the substrate is much more efficient as compared to other carbon atoms in the molecular backbones. In this sense, the τ_{CT} of refs 36 and 37 correspond presumably to $\tau_{thiolate}$ of our work even though the molecular backbones are different. Whereas the τ_{CT} could not be measured in the latter studies, it was concluded that τ_{CT} is much less than the C 1s core hole lifetime (6 fs)[72] for thiolate-bonded phenylene−ethylynenes[36] and is on the same time scale as the lifetime for thiolate-bonded terphenyl.[37] Note that assuming a hypothetical molecule, in which the nitrile group is directly attached to the thiolate moiety, a CT part of ca. 74% can be expected in the [N1s]π^* RAES spectrum for $\tau_{thiolate}$ = 2.3 fs. Under these conditions, the resonant part of the spectrum should be still large enough (26%) and clearly perceptible.

Along with taking τ_{CT} as derived from the experiment, a weighting of this parameter by E_{res} (see Table 1) can be considered in view of the theoretical expression for the molecular conductance, $G(n) = I/V = G_0 \exp(-\beta n)$, with the current I, the potential difference V, the quantum of conductance $G_0 = 2e^2/h$, and n and β as defined above.[73] Assuming $\beta = 1$[6] and setting $V = E_{res}$ (Table 1) and $I = e/\tau_{trans}$ with the electron charge e and the electron transfer rate $1/\tau_{CT}$,[31] we obtain "theoretical" estimates of τ_{CT} at 16.8, 54, and 206 fs for C2CN/Au, C3CN/Au, and C4CN/Au, respectively. Whereas the weighted τ_{CT} value for C2CN/Au is quite close to the experimental one, the new values for C3CN/Au and C4CN/Au are considerably higher. In spite of this difference, however, the dependence of the natural logarithm of τ_{CT} on n is again very close to the linear function, which is further evidence that the CT rate through the aliphatic chain is truly described by an exponential function. Note, however, that even in the case of the static conductance, an exact mechanism behind the exponential dependence of R on n is not fully understood. In particular, SAMs of aromatic thiols and isocyanides exhibit well-defined β parameters in spite of the considerable variation in the electronic structure of the assembled molecules with increasing length of the backbone.[18]

The values of β_{CT} (1.24/CH_2) and $\tau_{thiolate}$ (1.35 fs) associated with the modified (weighting by E_{res}) dependence of ln(τ_{CT}) on n are, respectively, higher and lower than the corresponding values for the nonweighted dependence. This might imply that the values of β_{CT} (0.93) and $\tau_{thiolate}$ (2.3 fs) associated with the latter case represent, respectively, the lower and upper limits for these parameters.

The exponential dependence of τ_{CT} on the number of methylene units along with the given value of the attenuation factor (β_{CT}) results in a comparably slow CT along the aliphatic chain. Even for such a short-chain molecule as C4CN it requires ca. 100 fs to transfer the electron from the tail group to the substrate. These slow transfer rates are considered to be the reason behind a variety of interesting phenomena in photoemission from SAMs, associated with electrostatic pinning of the energy states.[9,74−77] Indeed, the characteristic CT time along the aliphatic chain is significantly longer than the natural lifetime of the excited state in photoemission, so that the charge compensation of the photoemission hole occurs not during but long after the photoemission event. Due to this effect, depending on the exact situation, SAMs behave both as conductors and as insulators. In most cases, a standard description in terms of the chemical shift is fully adequate and sufficient, but in some selected situations, such as, e.g., evaporation of alkali metals on SAM substrate,[9,75] an embedded dipole layer,[74] or mixing molecules with different tail groups,[76,77] the insulating character of the SAMs, with electrostatic pinning of the associated energy states, comes to the foreground and not Fermi but vacuum-level alignment between the hydrocarbon matrix of the SAM and substrate occurs.

5. Conclusions

We applied resonant Auger spectroscopy within the framework of the core hole clock method to study the dynamics of CT processes in alkanethiolate SAMs on gold. For this purpose, we prepared a series of high-quality SAMs of nitrile-substituted alkanethiolates with variable length of the alkyl chain. Due to such a molecular architecture, the CT pathway was unambiguously defined (from the nitrile tailgroup, which could be resonantly excited by narrow bandwidth synchrotron radiation at the N K-edge, to the substrate over the alkyl chain and the thiolate−gold anchor). It was found that similar to the static conductance, the dependence of the CT time on the number of methylene units in the alkyl chain can be coarsely described by an exponential function with an attenuation factor of 0.93 per unit, which corresponds to 0.72 $Å^{-1}$ with respect to the length. As a result, the CT time is quite long even for a relatively short alkyl chain; in particular, it is ca. 100 fs for the chain consisting of only four CH_2 units. In contrast, the CT time associated with the thiolate headgroup anchor was found to be quite short, viz. 2.3 fs, which suggests that the thiolate−gold anchor provides an efficient interfacial electronic coupling between the aliphatic backbone and the substrate.

The advantages of the CHC method in its specific application to SAMs are, except for direct access to the dynamic characteristics of CT, a clear knowledge of the number of molecules participating in CT and the lack of contact problem, the molecules are "contacted" by an X-ray photon and behave individually. Nitrile, as used here, is seen to be a good candidate for CHC studies because of the suitable core hole lifetime and the large contrast between resonant and nonresonant core decay spectra, in particular, the large spectator shift. Extension to other functional groups is possible and promises to become a very valuable new source of information on CT dynamics in organic layers important for many applications, above all for future molecular electronics. Finally, not only a femtosecond but also an attosecond domain is accessible by CHC, which opens further perspectives.[78]

Acknowledgment. M.Z. thanks M. Grunze for support of this work, N. Ballav, F. Chesneau, V. Korolkov, and S. Rausch for help provided at different stages of this project, L. S. O. Johansson and E. Moons for technical cooperation, and the MAX-lab staff, A. Preobrajenski, in particular, for assistance during the experiments. This work was supported by DFG (ZH 63/14-1) and received funding from the European Community's Seventh Framework Programme (FP7/2007-2013) under grant agreement no. 226716. S.N. and P.F. acknowledge support by the Munich Centre for Advanced Photonics (project C.1.5.). D.L.A. and P.K. acknowledge partial support from the NSF Funded Center for Nanoscale Science (MRSEC DMR-0080019).

References and Notes

(1) Hagfeld, A.; Grätzel, M. *Chem. Rev.* **1995**, *95*, 49–68.
(2) Miller, R. J. D.; McLendon, G. L.; Nozik, A. J.; Schmickler, W.; Willig, F. *Surface Electron Transfer Processes*; VCH: New York, 1995.
(3) Itoh, N.; Stoneham, A. M. *Materials Modification by Electronic Excitation*; Cambridge University Press: Cambridge, 2001.
(4) Cahen, D.; Kahn, A. *Adv. Mater.* **2003**, *15*, 271–277.
(5) Nitzan, A.; Ratner, M. A. *Science* **2003**, *300*, 1384–1389.
(6) Adams, D. M.; Brus, L.; Chidsey, C. E. D.; Creager, S.; Creutz, C.; Kagan, C. R.; Kamat, P. V.; Lieberman, M.; Lindsay, S.; Marcus, R. A.; Metzger, R. M.; Michel-Beyerle, M. E.; Miller, J. R.; Newton, M. D.; Rolison, D. R.; Sankey, O.; Schanze, K. S.; Yardley, J.; Zhu, X. *J. Phys. Chem. B* **2003**, *107*, 6668–6697.
(7) Tour, J. M. *Molecular Electronics*; World Scientific: Singapore, 2003.
(8) Zhu, X.-Y. *Surf. Sci. Rep.* **2004**, *56*, 1–83.
(9) Ahn, H.; Zharnikov, M.; Whitten, J. E. *Chem. Phys. Lett.* **2006**, *428*, 283–287.
(10) Selzer, Y.; Allara, D. L. *Annu. Rev. Phys. Chem.* **2006**, *57*, 593–623, and references therein.
(11) Wold, D. J.; Haag, R.; Rampi, M. A.; Frisbie, C. D. *J. Phys. Chem. B* **2002**, *106*, 2813–2816.
(12) Fan, F. R. F.; Yao, Y.; Cai, L.; Cheng, L.; Tour, J. M.; Bard, A. J. *J. Am. Chem. Soc.* **2004**, *126*, 4035–4042.
(13) Engelkes, V. B.; Beebe, J. M.; Frisbie, C. D. *J. Am. Chem. Soc.* **2004**, *126*, 14287–14296.
(14) Lewis, P. A.; Inman, C. E.; Maya, F.; Tour, J. M.; Hutchison, J. E.; Weiss, P. S. *J. Am. Chem. Soc.* **2005**, *127*, 17421–17426.
(15) Tivanski, A. V.; He, Y.; Borguet, E.; Liu, H.; Walker, G. C.; Waldeck, D. H. *J. Phys. Chem. B* **2005**, *109*, 5398–5402.
(16) Akkerman, H. B.; Blom, P. W. M.; de Leeuw, D. M.; de Boer, B. *Nature* **2006**, *441*, 69–72.
(17) Moore, A. M.; Dameron, A. A.; Mantooth, B. A.; Smith, R. K.; Fuchs, D. J.; Ciszek, J. W.; Maya, F.; Yao, Y.; Tour, J. M.; Weiss, P. S. *J. Am. Chem. Soc.* **2006**, *128*, 1959–1967.
(18) Kim, B.-S.; Beebe, J. M.; Jun, Y.; Zhu, X.-Y.; Frisbie, C. D. *J. Am. Chem. Soc.* **2006**, *128*, 4970–4971.
(19) Park, H.; Park., J.; Kim, A. K. L.; Anderson, E. H.; Alivisatos, P. A.; McEuen, P. L. *Nature* **2000**, *407*, 57–60.
(20) Park, J.; Pasupathy, A. N.; Goldsmith, J. I.; Chang, C.; Yaish, Y.; Petta, J. R.; Rinkoski, M.; Sethna, J. P.; Abruna, H. D.; McEuen, P. L.; Ralph, D. C. *Nature* **2002**, *417*, 722–725.
(21) Selzer, Y.; Cabassi, M. A.; Mayer, T. S.; Allara, D. L. *J. Am. Chem. Soc.* **2004**, *126*, 4052–4053.
(22) Selzer, Y.; Cabassi, M. A.; Mayer, T. S.; Allara, D. L. *Nanotechnology* **2004**, *15*, S483–488.
(23) Selzer, Y.; Cai, L.; Cabassi, M. A.; Yao, Y.; Tour, J. M.; Mayer, T. S.; Allara, D. L. *Nano Lett.* **2005**, *1*, 61–65.
(24) Xu, B.; Xiao, X.; Yang, X.; Zang, L.; Tao, N. *J. Am. Chem. Soc.* **2005**, *127*, 2386–2387.
(25) Rampi, M. A.; Schueller, O. J. A.; Whitesides, G. M. *Appl. Phys. Lett.* **1998**, *72*, 1781–1783.
(26) Weiss, E. A.; Chiechi, R. C.; Kaufman, G. K.; Kriebel, J. K.; Li, Z.; Duati, M.; Rampi, M. A.; Whitesides, G. M. *J. Am. Chem. Soc.* **2007**, *129*, 4336–4349.
(27) Seitz, O.; Vilan, A.; Cohen, H.; Hwang, J.; Haeming, M.; Schoell, A.; Umbach, E.; Kahn, A.; Cahen, D. *Adv. Funct. Mater.* **2008**, *18*, 1–12.
(28) Lee, M. H.; Speyer, G.; Sankey, O. F. *Phys. Status Solidi B* **2006**, *243*, 2021–2029.
(29) Tarakeshhwar, P.; Palacios, J. J.; Kim, D. M. *IEEE Trans. Nanotechnol.* **2009**, *8*, 16–21.
(30) Beebe, J. M.; Engelkes, V. B.; Miller, L. L.; Frisbie, C. D. *J. Am. Chem. Soc.* **2002**, *124*, 11268–11269.
(31) Neppl, S.; Bauer, U.; Menzel, D.; Feulner, P.; Shaporenko, A.; Zharnikov, M.; Kao, P.; Allara, D. L. *Chem. Phys. Lett.* **2007**, *447*, 227–231.
(32) Brühwiler, P. A.; Karis, O.; Mårtensson, N. *Rev. Mod. Phys.* **2002**, *74*, 703–740.

(33) Campbell, J. L.; Papp, T. *At. Data Nucl. Data Tables* **2001**, *77*, 1–56.
(34) Schnadt, J.; Brühwiler, P. A.; Patthey, L.; O'Shea, J. N.; Södergen, S.; Odelius, M.; Ahuja, R.; Karis, O.; Bässler, M.; Persson, P.; Siegbahn, H.; Lunell, S.; Mårtenson, N. *Nature* **2002**, *418*, 620–623.
(35) de Jong, M. P.; Friedlein, R.; Sorensen, S. L.; Öhrwall, G.; Osikowicz, W.; Tengsted, C. *Phys. Rev. B* **2005**, *72*, 035448.
(36) Wang, L.; Chen, W.; Huang, C.; Chen, Z.-K.; Wee, A. T. S. *J. Phys. Chem. B* **2006**, *110*, 674–676.
(37) Chen, W.; Wang, L.; Huang, C.; Lin, T. T.; Gao, X. Y.; Loh, K. P.; Chen, Z. K.; Wee, A. T. S. *J. Am. Chem. Soc.* **2006**, *128*, 935–939.
(38) Ulman, A. *An Introduction to Ultrathin Organic Films: Langmuir-Blodgett to Self-Assembly*; Academic Press: New York, 1991. Ulman, A. *Chem. Rev* **1996**, *96*, 1533–1554.
(39) In *Thin films: self-assembled monolayers of thiols*; Ulman, A., Ed.; Academic Press: San Diego, CA, 1998.
(40) Love, J. C.; Estroff, L. A.; Kriebel, J. K.; Nuzzo, R. G.; Whitesides, G. M. *Chem. Rev.* **2005**, *105*, 1103–1169.
(41) Urquhart, G. G.; Gates, J. W.; Connor, R. *Org. Synth.* **1941**, *21*, 36–38.
(42) Frey, S.; Shaporenko, A.; Zharnikov, M.; Harder, P.; Allara, D. L. *J. Phys. Chem. B* **2003**, *107*, 7716–7725.
(43) Wirde, M.; Gelius, U.; Dunbar, T.; Allara, D. L. *Nucl. Instrum. Methods Phys. Res. B* **1997**, *131*, 245–251.
(44) Jäger, B.; Schürmann, H.; Müller, H. U.; Himmel, H.-J.; Neumann, M.; Grunze, M.; Wöll, Ch. *Z. Phys. Chem.* **1997**, *202*, 263–272.
(45) Heister, K.; Zharnikov, M.; Grunze, M.; Johansson, L. S. O.; Ulman, A. *Langmuir* **2001**, *17*, 8–11.
(46) Zharnikov, M.; Grunze, M. *J. Vac. Sci. Technol. B* **2002**, *20*, 1793–1807.
(47) *Surface chemical analysis-X-ray photoelectron spectrometers-Calibration of the energy scales*; ISO 15472:2001, 2006.
(48) Moulder, J. F.; Stickle, W. E.; Sobol, P. E.; Bomben, K. D. In *Handbook of X-ray Photoelectron Spectroscopy*; Chastian, J., Ed.; Perkin-Elmer Corp.: Eden Prairie, MN, 1992.
(49) Stöhr, J. *NEXAFS Spectroscopy*; Springer Series in Surface Science 25; Springer-Verlag: Berlin, 1992.
(50) Batson, P. E. *Phys. Rev. B* **1993**, *48*, 2608–2610.
(51) Zubavichus, Y.; Shaporenko, A.; Grunze, M.; Zharnikov, M. *J. Phys. Chem. A* **2005**, *109*, 6998–7000.
(52) Zubavichus, Y.; Shaporenko, A.; Korolkov, V.; Grunze, M.; Zharnikov, M. *J. Phys. Chem. B* **2008**, *112*, 13711–13716.
(53) Laibinis, P. E.; Whitesides, G. M.; Allara, D. L.; Tao, Y.-T.; Parikh, A. N.; Nuzzo, R. G. *J. Am. Chem. Soc.* **1991**, *113*, 7152–7167.
(54) Himmelhaus, M.; Gauss, I.; Buck, M.; Eisert, F.; Woll, Ch.; Grunze, M. *J. Electron Spectrosc. Relat. Phenom.* **1998**, *92*, 139–149.
(55) Heister, K.; Zharnikov, M.; Grunze, M.; Johansson, L. S. O. *J. Phys. Chem. B* **2001**, *105*, 4058–4061.
(56) Zharnikov, M. *J. Electron Spectrosc. Relat. Phenom.* **2010**, *178*−*179*, 380–393.
(57) Yang, Y. W.; Fan, L. J. *Langmuir* **2002**, *18*, 1157–1164.
(58) Ishida, T.; Choi, N.; Mizutani, W.; Tokumoto, H.; Kojima, I.; Azehara, H.; Hokari, H.; Akiba, U.; Fujihira, M. *Langmuir* **1999**, *15*, 6799–6806.
(59) Shaporenko, A.; Terfort, A.; Grunze, M.; Zharnikov, M. *J. Electron Spectrosc. Relat. Phenom.* **2006**, *151*, 45–51.
(60) Weidner, T.; Krämer, A.; Bruhn, C.; Zharnikov, M.; Shaporenko, A.; Siemeling, U.; Träger, F. *Dalton Trans.* **2006**, 2767–2777.
(61) Bagus, P. S.; Weiss, K.; Schertel, A.; Wöll, Ch.; Braun, W.; Hellwig, H.; Jung, C. *Chem. Phys. Lett.* **1996**, *248*, 129–135.
(62) Väterlein, P.; Fink, R.; Umbach, E.; Wurth, W. *J. Phys. Chem.* **1998**, *108*, 3313–3320.
(63) Hähner, G.; Kinzler, M.; Thümmler, C.; Wöll, Ch.; Grunze, M. *J. Vac. Sci. Technol.* **1992**, *10*, 2758–2763.
(64) Zharnikov, M.; Frey, S.; Heister, K.; Grunze, M. *Langmuir* **2000**, *16*, 2697–2705.
(65) Hautman, J.; Bareman, J. P.; Mar, W.; Klein, M. L. *J. Chem. Soc., Faraday Trans.* **1991**, *87*, 2031–2039.
(66) Sekitani, J.; Ikenaga, E.; Tanaka, H.; Mase, K.; Tanaka, K. *J. Electron Spectrosc. Relat. Phenom.* **1998**, *88*−*91*, 831–836.
(67) Rye, R. R.; Houston, J. E. *J. Chem. Phys.* **1981**, *75*, 2085–2090.
(68) Ortiz, J. V. *J. Chem. Phys.* **1985**, *83*, 4604–4617.
(69) Kempgens, B.; Kivimäki, A.; Neeb, M.; Köppe, H. M.; Bradschaw, A. M.; Feldhaus, J. *J. Phys. B* **1996**, *29*, 5389–5403.
(70) Slowinski, K.; Chamberlain, R. V.; Miller, C. J.; Majda, M. *J. Am. Chem. Soc.* **1997**, *119*, 11910–11919.
(71) Bumm, L. A.; Arnold, J. J.; Dunbar, T. D.; Allara, D. L.; Weiss, P. S. *J. Phys. Chem. B* **1999**, *103*, 8122–8127.
(72) Coville, M.; Thomas, T. D. *Phys. Rev. A* **1991**, *43*, 6053–6056.
(73) Tomfohr, J.; Sankey, O. F. *J. Chem. Phys.* **2004**, *120*, 1542–1554, and references therein.
(74) Cabarcos, O. M.; Shaporenko, A.; Weidner, T.; Uppili, S.; Dake, L. S.; Zharnikov, M.; Allara, D. L. *J. Phys. Chem. C* **2008**, *112*, 10842–10854.
(75) Ge, Y.; Weidner, T.; Ahn, H.; Whitten, J. E.; Zharnikov, M. *J. Phys. Chem. C* **2009**, *113*, 4575–4583.
(76) Ballav, N.; Terfort, A.; Zharnikov, M. *J. Phys. Chem. C* **2009**, *113*, 3697–3706.
(77) Venkataraman, N. V.; Zürcher, S.; Rossi, A.; Lee, S.; Naujoks, N.; Spencer, N. D. *J. Phys. Chem. C* **2009**, *113*, 5620–5628.
(78) Föhlisch, A.; Feulner, P.; Hennies, F.; Fink, A.; Menzel, D.; Sanchez-Portal, D.; Echenique, P. M.; Wurth, W. *Nature* **2005**, *436*, 373–376.

JP1042816